Supporting Search for the Standard Model Higgs Boson in Vector Boson Fusion Decaying via the $H \to WW^{(*)} \to \ell\nu\ell\nu$ Channel Using the Matrix Element Method

Matthew M. Bluteau

Acadia University, Wolfville NS and Simon Fraser University, Burnaby BC
098485b@acadiau.ca

Supervisor: Dr. Bernd Stelzer

Simon Fraser University, Burnaby BC
stelzer@sfu.ca

1 Introduction

This report presents the initial stages of the implementation of a Matrix Element (ME) Method, a multivariate analysis technique (MVA), in the search for the SM Higgs boson in the $H \to WW^{(*)} \to \ell\nu\ell\nu$ ($\ell = e, \mu$) channel with 2 jets where the Higgs boson has been produced via vector boson fusion. It is a continuation of the Matrix Element Method implementation summarized in the June 6, 2012 ATLAS Note by the MVA group [1]. It is an alternate technique to the cut-based analysis from which the current ATLAS results are derived; thus, the final objective is to provide a direct comparison of the ME Method and the cut-based analysis [6].

1.1 The Higgs Search

The current focus of High Energy Physics is and will be for some time the search and validation of the Standard Model (SM) Higgs Boson. This investigation has captured not just the minds of interested physicists but the general public with evidence for this provided by the large media focus on the announcement of July 4$^{\text{th}}$, 2012 [2]. In the presentations by the ATLAS and CMS collaborations, evidence was revealed for the existence of a SM like Higgs Boson particle, the Higgs Boson being the only particle predicted to exist by the SM yet to be experimentally confirmed. So much excitement surrounds this particle because it is the scalar boson predicted by the electroweak symmetry breaking mechanism in the SM, the mechanism that gives mass to all massive elementary particles, and the existence of this particle would confirm the validity of this mechanism [3–5]. Papers detailing the search for the Higgs boson from 2011 and following the July 4$^{\text{th}}$ announcement all point to excesses in the mass region around $m_H = 126$ GeV. The current ATLAS analysis excludes the SM Higgs boson at 95% Confidence Level (CL) in the mass range 111-600 GeV except in the range 122-131 GeV and reports an excess of events with significance 5.9σ in this region driven by the $H \to ZZ^{(*)} \to 4\ell$, $H \to \gamma\gamma$, and $H \to WW^{(*)} \to \ell\nu\ell\nu$ channels [6]. This result firmly proves the observation of a new neutral boson; however, there is still much to be done in examining the details of the properties of this particle, requiring analysis of more data. For instance, discriminating between the various couplings of the Higgs to bosons and fermions is essential to the determination of whether the discovered particle is in fact a SM Higgs Boson, and since the $H \to WW^{(*)} \to \ell\nu\ell\nu$

channel contains a exclusivley a coupling of the Higgs to vector bosons, it will be instrumental in verifying the nature of the discovery.

1.2 Vector Boson Fusion

Vector boson fusion ($qq' \to qq'H$, henceforth VBF) is the second highest production process for the Higgs boson as one can see from production cross sections in Figure 1. However, this is not necessarily the case when one searches for exclusive channels, and in fact for the 2-jet $H \to WW^{(*)} \to \ell\nu\ell\nu$ channel, VBF production dominates over gluon fusion (ggF) [6]. As such, this analysis will be restricted to processes involving VBF production. For completeness, the Feynman diagram for VBF is displayed in Figure 2, and one can observe the flavour change of the incoming and outgoing quarks depending on the intermediate vector boson that mediates the process.

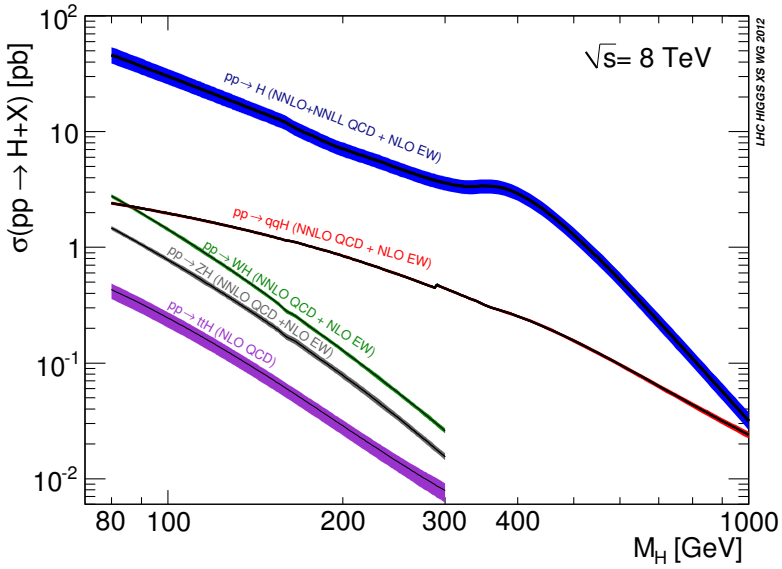

Figure 1: Standard Model Higgs boson production cross sections. Transition for VBF at M_H=300 GeV is due to change from ZWA (zero-width-approximation) to complex-pole-scheme [7, 8].

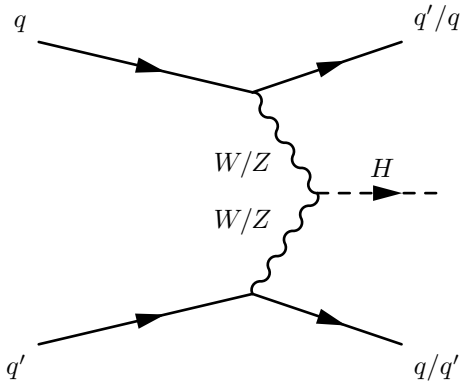

Figure 2: Feynman Diagram for VBF Higgs Boson Production

1.3 2-jet $H \to WW^{(*)} \to \ell\nu\ell\nu$ Channel

In general, the sensitivity of the $H \to WW^{(*)} \to \ell\nu\ell\nu$ decay channel is expected to be quite good compared to others owing to the high branching ratio of the $H \to WW^{(*)}$ mode [7, 8]; however, the mass resolution of the channel is hindered by the fact that there are neutrinos in the final state which escape the ATLAS detector undetected, meaning the system is kinematically under-constrained. Specifiying that the production process for this general channel be VBF, one gets the 2-jet $H \to WW^{(*)} \to \ell\nu\ell\nu$ channel pictured in the Feynman diagram in Figure 3. This diagram yields the matrix element for this process, and the use of the matrix element will be explained in Section 2.

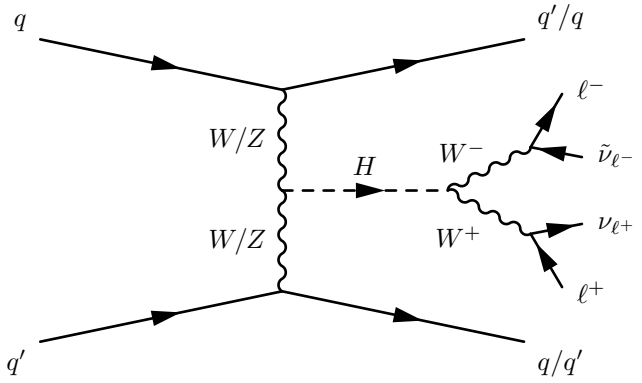

Figure 3: Feynman Diagram / Matrix Element for $H \to WW^{(*)} \to \ell\nu\ell\nu$ + 2 jet signal.

In contrast to the current cut-based analysis performed by the ATLAS collaboration, all possible final states with leptons from the first two generations will be included as part of the signal (*i*.e. $\ell = e, \mu$) but the incoming partons used in the matrix element will be limited to the two that yield the greatest cross section. In order to simplify the current analysis, the matrix element with the greatest cross section was determined using MadGraph/MadEvent 5 [9]. The matrix element calculations were generated with MadGraph 5 using the general input, `p p > h j j, h > w+ w- > e- ve~ e+ ve`, and then 10000 MC events were run using MadEvent 5 to determine the overall cross section. Because of the inner structure of MadGraph 5, the contributions of the most dominant matrix elements / diagrams had to be determined by first identifying the dominant integration channels and then splicing each into contributions from individual diagrams. The results of this exercise for the top 13 processes are summarized in Table 1.

Based on these results, the top two subprocesses in Table 1 were selected since they are actually mirror processes and differ only by the intermediate vector bosons as one can verify by looking at Figure 3 (in essence, one gets two subprocesses for one MadGraph input: `u d > h u d, h > l- vl~ l+ vl`). Evidently, a future improvement of this analysis will be to expand the number of inputs and thus matrix elements since this matrix element only accounts for approximately 32% of the total 2-jet $H \to WW^{(*)} \to \ell\nu\ell\nu$ channel cross section (relative to exclusive VBF production); however, the kinematic differences between these matrix elements is expected to be small because the PDF will not change the transverse observables (only the longitudinal boost).

1.3.1 Kinematics

Because the Matrix Element method is based on first principles (as explained later), it utilizes all kinematic information for a given process; as such, it is useful to look at the kinematic distributions of the final state parton-level particles. To achieve this, 10 000 events were generated using MadGraph/MadEvent, and following some conversions and extraction, the distributions shown

Table 1: Summary of Cross Section Contributions to General p p → h j j Process (x = e- ve e+ ve˜).

Process	**Fractional Contribution to Total X-Section**
u d → x u d	0.1675
d u → x u d	0.149
c˜u → x d s˜	0.044
u s → x c d	0.0439
s u → x c d	0.0338
u d˜→ x u d˜	0.0304
u u˜→ x d d˜	0.0295
u c˜→ x d s˜	0.0292
u˜u → x d d˜	0.0273
u d˜→ x c s˜	0.0267
d˜u → x c s˜	0.0267
s˜u˜→ x c˜d˜	0.0252
˜u → x u d˜	0.0235
Sum	0.6567

in Figure 4 were created. One kinematic characteristic observable from these distributions is the forwardness of the final state jets that both have peaks at a magnitude of approximately 3. Another important observation is the small values of $\Delta\phi_{\ell\ell}$in Figure 4 (e). This is a direct result of the fact that the SM Higgs boson is spin-0 and undergoes a parity violating weak decay which induces a spin correlation between the final state leptons.

1.4 Background Process

The primary background process for the channel under consideration is $t\bar{t}$ production. As seen in Figure 5, the top quarks decay leptonically via the weak interaction producing the same similar state as the proposed signal. It is important to note that b quark jets are produced almost exclusively for this process, and thus b-tagging algorithms are extremely important for the identification of the background sample.

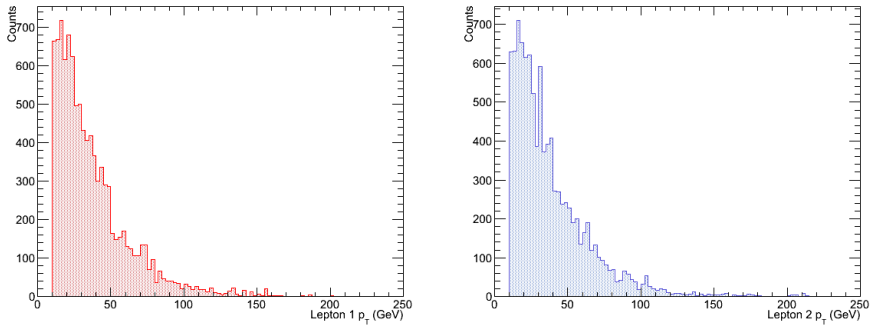

(a)

(b)

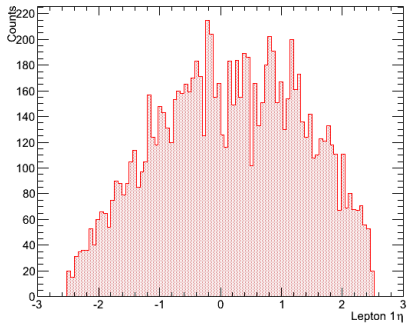

(c)

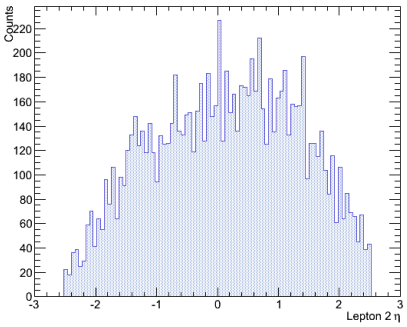

(d)

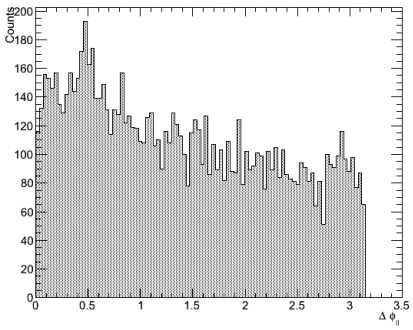

(e)

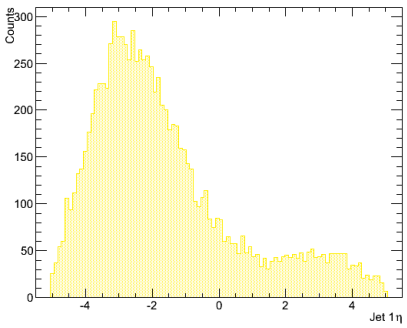

(f)

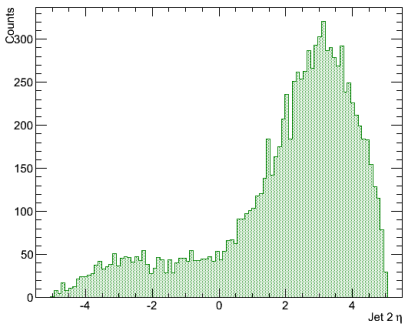

(g)

Figure 4: Kinematic distributions of MadEvent generated events for the signal hypothesis showing (a) first lepton p_T, (b) second lepton p_T, (c) first lepton pseudorapidity, η, (d) second lepton pseudorapidity, η, (e) difference in angle ϕ between the two leptons, (f) first jet pseudorapidity, η, (g) second jet pseudorapidity, η.

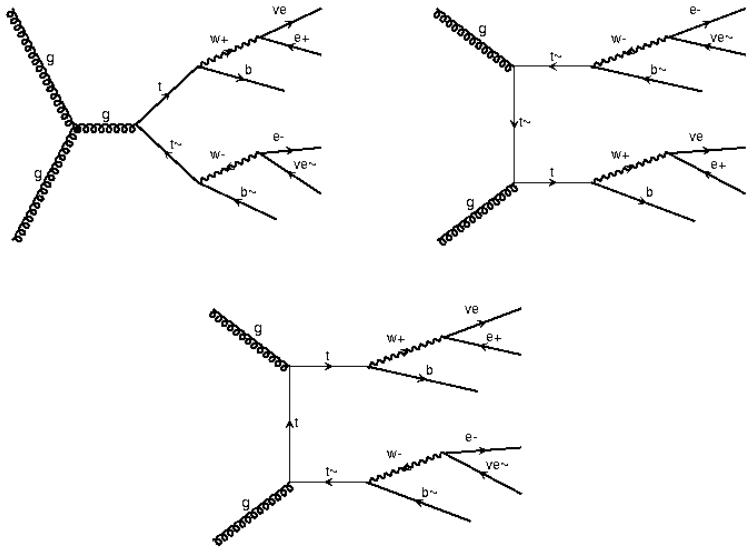

Figure 5: Matrix Elements / Feynman Diagrams for Dominant $t\bar{t}$ Background

2 Matrix Element Method

2.1 Theory Introduction

The ultimate goal of the Matrix Element method is to construct a event probability density function, P_{sample}, that describes the probability of observing an event in a given detector under a given hypothesis [10]. This density is constructed from the theory specified differential cross-sections of the relevant processes; hence, it is a technique which derives directly from first principles. In this analysis, pre-cut MC signal and background events are each tested for both the SM Higgs signal and background hypotheses. This is done by evaluating the event probability densities for the signal and background processes for each data sample as described below. Once these distributions have been obtained (four in total), an event probability discriminant (EPD) can be derived for each data sample. The EPD is defined as:

$$EPD(M_H) = \frac{P_H(M_H)}{P_H(M_H) + \sum_i P_{bkg_i}} \quad , \tag{1}$$

where P_{bkg_i} is the event probability density for background process i and $P_H(M_H)$ is the event probability density for the Higgs process with mass hypothesis m_H. As noted previously, only the $t\bar{t}$ background is considered in the current analysis, so the above sum will only be one term. The EPD is a useful quantity because it ranks events in a 1-D distribution based on whether they are signal or background like, meaning the EPD can be cut on.

2.2 Defining the Event Probability Density [1]

The total differential cross-section for a process is given by [11]:

$$d\sigma = \frac{(2\pi)^4 |M|^2}{4\sqrt{(q_1 \cdot q_2)^2 - m_{q_1}^2 m_{q_2}^2}} \, d\Phi_n(q_1 + q_2; p_1, .., p_n) \tag{2}$$

where $|M|$ is the Lorentz invariant matrix element calculated from the Feynman diagrams shown above; q_1, q_2 and m_{q_1}, m_{q_2} are the four momenta and masses of the incident particles; and $d\Phi_n$ is the n-body phase space given by:

$$d\Phi_n(q_1+q_2;p_1,..,p_n) = (2\pi)^4\delta^4(q_1+q_2-\sum_{i=1}^{n}p_i)\prod_{i=1}^{n}\frac{d^3p_i}{(2\pi)^3 2E_i}. \tag{3}$$

The event probability density for process α, P_α, is defined as:

$$P_\alpha = \frac{1}{\sigma}\sum_{i,j}\int\frac{d\sigma_{ij}(y,\alpha)}{dy}T(x,y)dy \quad . \tag{4}$$

$T(x,y)$ is the transfer function which describes the probability of measuring x in the detector given the generator level final state y. For the present analysis, a δ function is used for leptons and jet angular resolution (because they are assumed to be well measured and close to truth values), a uniform distribution for the neutrinos, and a double gaussian for jet energy resolution defined by:

$$T_{jet}(E_{parton},E_{jet}) = \frac{1}{\sqrt{2\pi}(p_2+p_3p_5)}(exp\frac{-(\delta_E-p_1)^2}{2p_2^2}+p_3\ exp\frac{-(\delta_E-p_4)^2}{2p_5^2}) \quad . \tag{5}$$

The differential cross section, $\frac{d\sigma_{ij}(y,\alpha)}{dy}$, in Equation 4 is given by:

$$\frac{d\sigma_{ij}(y,\alpha)}{dy} = \int d\Phi\frac{|M_{ij}(\alpha)|^2 f_i(x_i,Q^2)f_j(x_j,Q^2)}{8x_ix_jE_{beam}^2}. \tag{6}$$

The variables in the previous two expressions are defined as follows:

- α is the process type
- i,j are the possible combinations of initial state partons
- x is the four-vector of the measured reconstructed final state
- y is the four-vector of the true final state at generator level
- $T(x,y)$ is the transfer function to describe expected measured kinematics x given true kinematics y
- $M_{ij}(\alpha)$ is the matrix element for partons in initial states i and j
- $f_x(x_n,Q^2)$ are the parton distribution functions, taken from the CTEQ6L library
- x_n is the fraction of proton momentum carried by initial state parton n
- E_{beam} is the beam energy, which is taken as 7 TeV in this case
- $d\Phi$ represents the integral over N body phase space

Upon applying energy and momentum conservation and assuming a δ-function resolution for the lepton transfer functions, the differential cross section for an event with an ℓ,ν final state at leading order reduces to:

$$\frac{d\sigma_{ij}(y,\alpha)}{dy} = \sum_{i,j}\int\frac{|M_{ij}(\alpha)|^2 f_i(x_i,Q^2)f_j(x_j,Q^2)}{16(2\pi^3)^8 16x_ix_jE_{beam}^2}\frac{dp_x^{\nu_1}dp_y^{\nu_1}dp_z^{\nu_1}dp_z^{\nu_2}}{E_{l_1}E_{l_2}E_{\nu_1}E_{\nu_2}} \tag{7}$$

A visual summary of the overall strategy for an individual event probability calculation is provided in Figure 6.

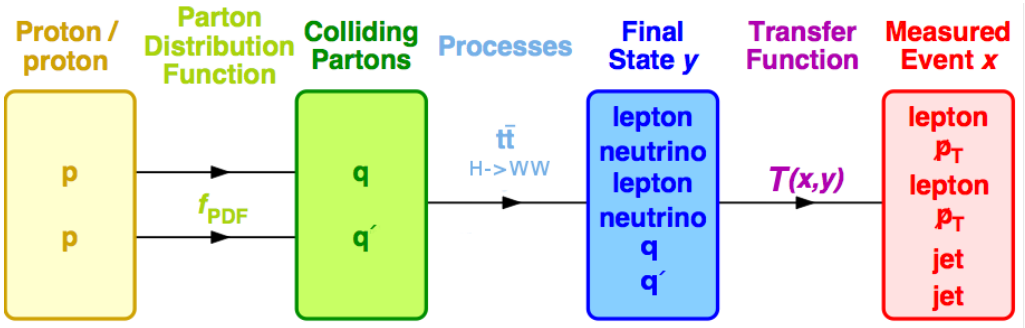

Figure 6: Schematic of an individual event probability calculation defined by Equation 4 [12]

2.3 Implementation

The matrix elements for signal and background, $M_{ij}(\alpha)$, were calculated using MadGraph [9] and, as mentioned previously, can be seen in Figures 3 and 5 for signal and background respectively. The integration steps necessary to obtain the event probability density (Equation 4) for each measured final state were performed numerically using the MadGraph add-on, MadWeight [13], which employs the adaptive Monte Carlo integrator VEGAS. Because of a current fault in the MadWeight functionality, the possible final dilepton states need to be specified explicitly when creating the matrix elements in MadGraph (*i.e.* "`l`" cannot be used to specify a range of possible leptons). The possible final states are $[e^+ \quad \nu_e \quad e^- \quad \tilde{\nu}_e]$, $[e^+ \quad \nu_e \quad \mu^- \quad \tilde{\nu}_\mu]$, $[\mu^+ \quad \nu_\mu \quad e^- \quad \tilde{\nu}_e]$, $[\mu^+ \quad \nu_\mu \quad \mu^- \quad \tilde{\nu}_\mu]$. Hence, matrix elements for both singal and background processes were generated with theses possible final states, and then signal and background MC samples were run through MadWeight for all possible cases, yielding the desired event probability density distributions seen below.

3 Preliminary Results

The event probability distributions for all possible signal/background cases are shown in Figure 7. From these figures, one can observe already a good separation between the MC signal and background samples.

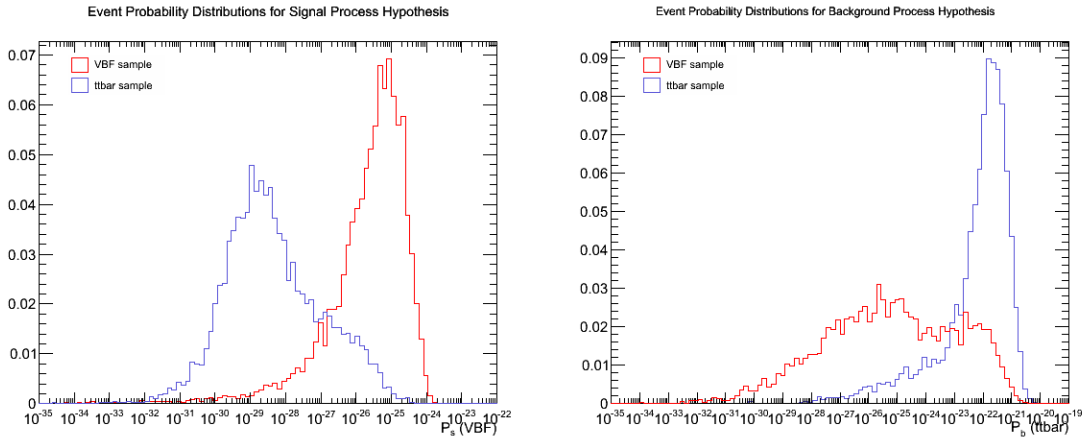

(a) Signal Hypothesis Distributions

(b) Background Hypothesis Distributions

Figure 7: Event Probability Densities for Signal and Background Samples

The good separation between signal and background samples is further reinforced by a 2 dimensional plot of the event probabilities in Figure 8 and histograms using 50 bins of both EPD distributions in Figure 9.

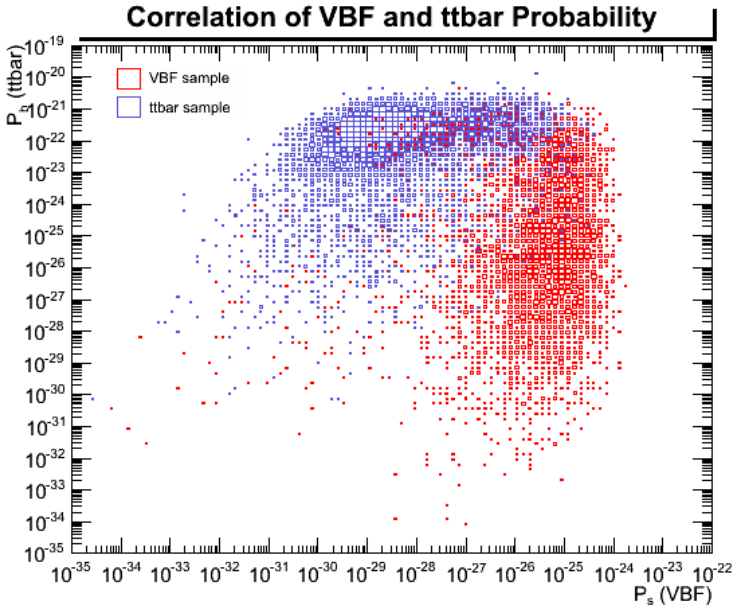

Figure 8: 2D Event Probability Plot

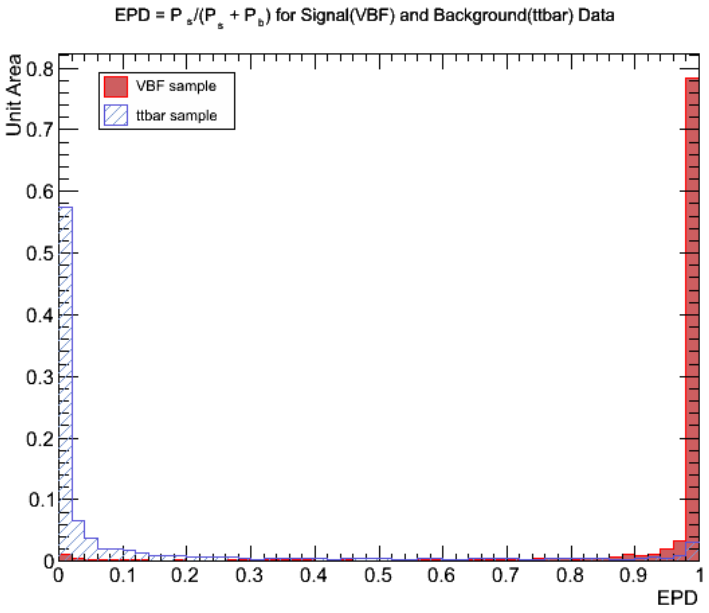

Figure 9: Raw EPD Distributions

Armed with the two EPD's, it is possible to cut on these distributions and compare to the more "simple" cut-based analysis. The variable used to compare these two approaches is the signal sensitivity, S_{sig} defined as:

$$S_{sig} = \frac{N_{sig}}{\sqrt{N_{bg}}} \quad . \tag{8}$$

The N's in Equation 8 represent the number of events and are obtained by integrating over the EPD distributions after applying the appropriate cuts. In order to do this in a logical manner, S_{sig} was first obtained for the current ATLAS cut-based analysis [6]. The most important cuts applied were as follows:

- A weighting of each event via the product of the pileup event weight and the Monte Carlo event weight (pileupEventWeight_090 * mcEventWeight_reco).
- $\Delta\phi_{\ell\ell} < 1.8$
- $\mathbf{p}_{\mathrm{T}}^{\mathrm{tot}} < 30$ GeV
- $m_{jj} > 500$ GeV
- $|\ \Delta y_{jj}\ | > 3.8$

Upon obtaining N_{sig} and N_{bg} for this cut-based analysis, the cut directly on the EPD distributions was applied such that the N_{bg}'s were approximately equal for both analyses. The final results of these steps are summarized in Table 2. It is important to note that these N's are based purely on the MC sample sizes used and have not been normalized to the expectation of a particular ATLAS dataset, but this limitation is eliminated by taking the ratio of the sensitivities, S_{sig}, for each analysis method (essentially cancelling out the normalization factor that would be applied to each N).

Using the signal sensitivities, S_{sig}, from Table 2, one finds that the EPD based analysis provides a 190% improvement over the simple cut based analysis that is currently published by ATLAS.

Table 2: Summary of ME Sensitivity Results

Quantity	**Current ATLAS Cuts**	**EPD Cut**
N_{sig}	1296.19	2463.95
N_{bg}	10.99	11.07
$N_{sig}/\sqrt{N_{bg}}$	390.97	740.48

4 Conclusion

This report provides a sound basis for further analysis of the $H \to WW^{(*)} \to \ell\nu\ell\nu$ 2-jet channel using the Matrix Element Method. Using the even probability distributions generated by MadWeight and the EPD for both signal and background samples, an improvement of 190% was seen in signal sensitivity over the current ATLAS cut-based analysis. Although this is encouraging to see, there is much more that can be done to improve this analysis. Immediate improvements are including more possible incoming partons, running more events from the background sample to increase the statistics, formulating a concurrent systematic uncertainty estimate, and evaluating the matrix elements and EPD for all possible background processes. In addition, some work has also been done in implementing this analysis within a standalone code that uses the matrix elements generated by MadGraph but provides more flexibility in implementation (compared to MadWeight).

References

[1] The ATLAS Collaboration, *Search for the Standard Model Higgs boson in the $H \to WW^{(*)} \to \ell\nu\ell\nu$ decay mode using Multivariate Techniques with 4.7 fb^{-1} of ATLAS data at $\sqrt{s}$ = 7 TeV*, ATLAS-CONF-2012-060 (2012), `https://atlas.web.cern.ch/Atlas/GROUPS/PHYSICS/CONFNOTES/ATLAS-CONF-2012-060/`.

[2] CERN, "Latest update in the search for the Higgs Boson (presentation)," July 4 2012, `https://cdsweb.cern.ch/record/1459565`.

[3] P.W. Higgs, Phys. Rev. Lett. **13** (1964) 508.

[4] F. Englert and R. Brout, Phys. Rev. Lett. **13** (1964) 321.

[5] G. S. Guralnik, C. R. Hagen, and T. W. B. Kibble, Phys. Rev. Lett. **13** (1964) 585.

[6] ATLAS Collaboration, *Observation of a New Particle in the Search for the Standard Model Higgs Boson with the ATLAS Detector at the LHC*, submitted to Phys. Lett. B (2012), `arXiv:1207.7214v1 [hep-ex]`.

[7] LHC Higgs Cross Section Working Group, S. Dittmaier, C. Mariotti, G. Passarino, and R. Tanaka (Eds.), *Handbook of LHC Higgs Cross Sections: 1. Inclusive Observables*, CERN-2011-002 (CERN, Geneva, 2011), `arXiv:1101.0593 [hep-ph]`.

[8] LHC Higgs Cross Section Working Group, S. Dittmaier, C. Mariotti, G. Passarino, and R. Tanaka (Eds.), *Handbook of LHC Higgs Cross Sections: 2. Differential Distributions*, CERN-2012-002 (CERN, Geneva, 2012), `arXiv:1201.3084 [hep-ph]`.

[9] J. A. et al., MadGraph *5: Going Beyond*, JHEP **128** (2011) 1106.

[10] Aaltonen, T. and others (CDF), *Measurement of the Single Top Quark Production Cross Section at CDF*, Phys. Rev. Lett., **101** (2008) 252001.

[11] K. Nakamura, et. al.,*The Review of Particle Physics*, J. Phys. G, **37** (2010), 075021.

[12] F. Fiedler et al., *The Matrix Element Method and its Application to Measurements of the Top Quark Mass*, `arXiv:1003.1316v2 [hep-ex]`.

[13] Pierre Artoisenet et al., *A*utomation of the matrix element reweighting method, `arXiv:1007.3300 [hep-ph]`.